

G328.4+0.2: A LARGE AND LUMINOUS CRAB-LIKE SUPERNOVA REMNANT

B. M. GAENSLER^{1,5}, J. R. DICKEL^{2,3} AND A. J. GREEN⁴*(To appear in The Astrophysical Journal)*

ABSTRACT

We report on radio continuum and H I observations of the radio source G328.4+0.2 using the Australia Telescope Compact Array. Our results confirm G328.4+0.2 to be a filled-center nebula with no surrounding shell, showing significant linear polarization and an almost flat spectral index. These results lead us to conclude that G328.4+0.2 is a Crab-like, or “plerionic”, supernova remnant (SNR), presumably powered by an unseen central pulsar. H I absorption towards G328.4+0.2 puts a lower limit on its distance of 17.4 ± 0.9 kpc, making it the largest ($D = 25$ pc) and most luminous ($L_R = 3 \times 10^{35}$ erg s⁻¹) Crab-like SNR in the Galaxy. We infer G328.4+0.2 to be significantly older than the Crab Nebula, but powered by a pulsar which is fast spinning ($P < 20$ ms) and which has a comparatively low magnetic field ($B < 10^{12}$ G). We propose G328.4+0.2, G74.9+1.2 and N157B as a distinct group of large-diameter, high-luminosity Crab-like SNRs, all powered by fast-spinning low-field pulsars.

Subject headings: ISM: individual (G328.4+0.2, G74.9+1.2, N157B) – ISM: supernova remnants – pulsars: general – radio continuum: ISM

1. INTRODUCTION

When a massive star ends its life in a supernova explosion, the outer layers of the star are expelled at high velocity, and interact with the ambient interstellar medium (ISM) to produce a supernova remnant (SNR). “Shell” SNRs are usually characterized by radio synchrotron emission with a limb-brightened morphology, roughly centered on the site of the supernova explosion. Some SNRs are classified as “composite”, indicating that as well as a shell they have an additional central component, characterized by a filled-center morphology, a flat spectral index ($-0.3 \lesssim \alpha \lesssim 0$; $S_\nu \propto \nu^\alpha$) and significant linear polarization. This extra component is usually interpreted as a synchrotron nebula, powered by a pulsar also formed in the supernova explosion (Milne et al. 1979; Weiler & Panagia 1980; Reynolds & Chevalier 1984). Thus even when a pulsar itself is not detected (as is the case much more often than not), the mere existence of one of these synchrotron nebulae tells us that an energetic pulsar must be located within.

The best known example of a pulsar-powered nebula is the Crab Nebula. However, it has long been apparent that the Crab is very different from most other SNRs, in that it consists of a synchrotron nebula and associated pulsar, but has *no* surrounding shell corresponding to the supernova blast wave. It is now recognized that about 5% of all SNRs similarly lack shells; these sources are generally referred to as “Crab-like” SNRs, or “plerions” (Weiler & Panagia 1978). It is still an open question as to whether Crab-like SNRs have surrounding shells which are simply not detectable (Chevalier 1977; Sankrit & Hester 1997), or whether they are fundamentally different from other SNRs in that they have no shell, invisible or otherwise (Nomoto 1987; Wallace, Landecker, & Taylor 1997).

Crab-like SNRs are thus important to identify and study, both for understanding the nature and evolution of SNRs, and because they are an unambiguous indication of the presence of

a young pulsar. The source G328.4+0.2 (MSH 15–57; Mills, Slee, & Hill 1961) has been the subject of several radio studies (Shaver & Goss 1970; Caswell et al. 1980; Whiteoak & Green 1996), which have indicated a featureless filled-center appearance and a comparatively flat spectral index. These properties have resulted in G328.4+0.2 being proposed as a member of the Crab-like class of SNRs, and indeed is the only Galactic Crab-like SNR easily accessible to Southern hemisphere observers. H I measurements with a two-element interferometer have shown H I absorption in this direction to a distance in excess of 20 kpc (Caswell et al. 1975). This large distance would make the SNR extraordinary luminous, even brighter than the Crab Nebula itself.

However, previous images of this source have been of only intermediate resolution (the best observations to date had only six beams across the SNR), while the lack of imaging capability in the H I measurements of Caswell et al. (1975) mean that the absorption they saw could have been coming from another bright source in the vicinity, rather than from the SNR itself. We therefore present new radio observations of G328.4+0.2 both in polarimetric continuum and in the H I line, aimed at confirming the Crab-like nature of this source, verifying the large distance claimed for it, and studying it at much higher resolution and sensitivity than in previous work. Our observations and analysis are described in §2, and our results are presented in §3. In §4 we confirm G328.4+0.2 as a Crab-like SNR, and infer the properties of the central pulsar presumed to be powering it. A complementary study of this source in X-rays is reported in a companion paper by Hughes, Slane & Plucinsky (2000).

2. OBSERVATIONS AND DATA REDUCTION

Our observations of G328.4+0.2 were made with the Australia Telescope Compact Array (ATCA; Frater, Brooks, & Whiteoak 1992), a 6 km east-west synthesis array located near Narrabri, NSW, Australia, on dates as listed in Table 1. Con-

¹Center for Space Research, Massachusetts Institute of Technology, 70 Vassar Street, Cambridge, MA 02139; bmg@space.mit.edu

²Astronomy Department, University of Illinois, 1002 West Green Street, Urbana, IL 61801; johnd@astro.uiuc.edu

³Netherlands Foundation for Research in Astronomy, PO Box 2, 7900 AA Dwingeloo, The Netherlands

⁴Astrophysics Department, University of Sydney, NSW 2006, Australia; a.green@physics.usyd.edu.au

⁵Hubble Fellow

tinuum observations were made at 1.4 and 4.5 GHz; each band had a width of 128 MHz, divided into 32 channels. Simultaneous with the 1.4 GHz data, observations were made in the H I line, centered on 1421 MHz and using 512 channels across a 4 MHz bandwidth. All four Stokes parameters (XX , YY , XY and YX) were recorded in continuum observations; only XX and YY were obtained in the H I line. All observations consisted of a single pointing centered on G328.4+0.2. Flux density calibration was carried out using observations of PKS B1934–638 (with assumed flux densities of 14.9 and 6.3 Jy at 1.4 and 4.5 GHz respectively), while antenna gains and polarization were calibrated using regular observations of MRC B1456–367 at 1.4 GHz and PMN J1603–4904 at 4.5 GHz.

Data were reduced in the MIRIAD package. After flagging and calibration were carried out, total intensity images were formed at each of 1.4 and 4.5 GHz using uniform weighting, multi-frequency synthesis and maximum entropy deconvolution. The resulting images were then corrected for the mean primary beam response, with resolutions and sensitivities given in Table 1.

Images in linear polarization were formed by creating separate images in Stokes Q and U , deconvolving each of these separately using the CLEAN algorithm, and then combining with appropriate debiasing to form $L = (Q^2 + U^2)^{1/2}$. At 1.4 GHz, significant Faraday rotation across the band can depolarize the emission, and images of linear polarization were produced on a channel by channel basis and then averaged to form a single map. At 4.5 GHz, differential Faraday effects are negligible and the entire observing bandwidth was used to form a single pair of Stokes Q and U images. The resulting maps of linear polarization were clipped wherever Stokes I , Q or U fell below 3σ .

For the H I data, the continuum contribution was subtracted in the u - v plane (van Langevelde & Cotton 1990), and a cube then formed using uniform weighting and discarding all baselines longer than $7 \text{ k}\lambda$. The cube contained planes between -200 km s^{-1} and $+200 \text{ km s}^{-1}$ (LSR) at intervals of 4 km s^{-1} . The peak flux density in the image was sufficiently low that no sidelobes were apparent, and no attempt was made to deconvolve. The cube was then weighted by the corresponding 1.4 GHz continuum image. Absorption spectra against SNR G328.4+0.2 and the nearby H II region G328.30+0.43 were then generated by integrating over an appropriate spatial region and renormalizing appropriately to give units of fractional absorption.

The rms noise, σ , in each absorption spectrum was estimated from the fluctuations in line-free channels. As in previous papers (e.g. Gaensler, Manchester, & Green 1998), we adopt 6σ as a threshold for significance, to take into account the increase in system temperature of the receivers due to the brightness temperature of H I in the Galactic Plane.

3. RESULTS

3.1. Continuum

Images of G328.4+0.2 at 1.4 and 4.5 GHz are shown in Fig 1, and properties of the source at each frequency are given in Table 1. The source is approximately circular, with a bar-like feature running east-west at the peak of the emission. A plateau of fainter emission surrounds this bar; this plateau is significantly more pronounced to the east and to the south.

G328.4+0.2 is of sufficiently small diameter that its entire flux density is recovered by the telescope at both observing frequencies, and the corresponding flux densities (after a

background correction has been applied) are given in Table 1. These flux densities, together with the 0.8 GHz measurement of Whiteoak & Green (1996), imply a spectral index for the source $\alpha = -0.12 \pm 0.03$.

Examination of the whole 1.4 GHz field (not shown here) shows there to be no outer shell of emission surrounding G328.4+0.2, out to a radius of 15 arcmin and down to a 1σ sensitivity of $0.8 \text{ mJy beam}^{-1}$, corresponding to a surface brightness limit at 1 GHz (assuming a typical shell spectral index $\alpha = -0.5$) of $\Sigma = 1.6 \times 10^{-21} \text{ W m}^{-2} \text{ Hz}^{-1} \text{ sr}^{-1}$.

Discarding the shortest baselines to filter out extended emission, we can put 5σ limits at 1.4 GHz and 4.5 GHz of 7 and 0.3 mJy respectively on the flux density of any point source within G328.4+0.2.

3.2. Polarization

At 1.4 GHz, the only linearly polarized emission seen from G328.4+0.2 is in a couple of clumps seen at the position of the peak in total intensity. These clumps have a fractional polarized intensity of $\sim 1\%$. When imaged on a channel by channel basis, the variation of the position angle of this polarization, ϕ , shows a $\phi \propto \lambda^2$ dependence across the 1.4 GHz band. This allows us to determine a rotation measure (RM) for this emission (cf. Gaensler, Manchester, & Green 1998) of $-900 \pm 100 \text{ rad m}^{-2}$, where the uncertainty is dominated by spatial variations in RM rather than by uncertainty in the measurement process (for which typical uncertainties are $\pm 30 \text{ rad m}^{-2}$).

At 4.5 GHz, significantly more linear polarization is seen from G328.4+0.2, with a spatial distribution shown in Fig 2. Although the polarization appears to be reduced around the edges of the source, this is most likely an artifact of the clipping of polarized emission below 3σ in Stokes Q and U ; the fractional polarized intensity shows no decrease towards the edges. The level of fractional polarization ranges between 5% and 50% with a mean of 20%.

An RM of 1000 rad m^{-2} corresponds to $\Delta\phi \approx 10^\circ$ across the entire 4.5 GHz observing bandwidth, which is smaller than the uncertainties in position angles of individual frequency channels. Thus no rotation measures could be extracted from the 4.5 GHz data.

3.3. H I absorption

H I absorption towards G328.4+0.2 needs to be compared to an H I emission spectrum in a similar part of the sky. But because most of the power in H I emission is on scales larger than were sampled by our observations, such a spectrum is difficult to extract from our ATCA data. Instead, we use an H I emission spectrum taken from the single-dish survey of Kerr et al. (1986), in the direction $l = 328.^\circ 5$, $b = 0.^\circ 25$. This emission profile is shown in the upper panel of Fig 3. Two ATCA absorption profiles are also shown in Fig 3: towards G328.4+0.2 and towards the H II region G328.30+0.43, 15 arcmin to the north-west. The latter emits in various maser lines, and is known to have a systemic velocity of approximately -95 km s^{-1} (Braz & Epchtein 1983; Cohen, Masheder, & Caswell 1995).

At negative velocities, the two spectra are very similar, and match well the H I emission seen along similar lines-of-sight. However, a significant difference is seen at positive velocities, where H I at a velocity of $+28 \text{ km s}^{-1}$ is clearly producing significant absorption against G328.4+0.2, but only a weak feature is seen for G328.30+0.43. Examination of the image plane corresponding to this velocity clearly shows the outline of all of G328.4+0.2 in absorption, leaving no doubt that this absorption

feature is genuine. However, for the H II region G328.30+0.43 we see no real match in absorption to the source's morphology at this velocity, as expected given that it is known to be at the tangent point. This weak absorption probably corresponds to fluctuations in the H I emission at this velocity, appearing negative because of spatial filtering by the interferometer.

4. DISCUSSION

4.1. Distance

The H I spectrum shown in Fig 3 demonstrates clearly that the systemic velocity of G328.4+0.2 is at least $+28 \text{ km s}^{-1}$. H I emission is seen at $+28 \text{ km s}^{-1}$ not just in the direction of G328.4+0.2, but towards several other sources in the vicinity (Caswell et al. 1975). Thus it is unlikely that the emission and absorption seen at this velocity correspond to some much closer cloud of gas which deviates dramatically from the Galactic rotation curve. While an H I emission feature at $+58 \text{ km s}^{-1}$ shows no corresponding absorption, its low brightness temperature means that we can probably not use this result to derive an upper limit on the source's radial velocity.

To calculate a lower limit on the distance to G328.4+0.2, we adopt standard IAU parameters for the Sun's orbital velocity ($\Theta_0 = 220 \text{ km s}^{-1}$) and distance from the Galactic Centre ($R_0 = 8.5 \text{ kpc}$) (Kerr & Lynden-Bell 1986), use the best fitting model for Galactic rotation of Fich, Blitz & Stark (1989), and assume uncertainties in systemic velocities of $\pm 7 \text{ km s}^{-1}$. For a systemic velocity of $+28 \text{ km s}^{-1}$, it then follows that G328.4+0.2 must be at a distance of at least $17.4 \pm 0.9 \text{ kpc}$. In further discussion, we assume a distance $d = 17d_{17} \text{ kpc}$; the diameter of G328.4+0.2 is then $25d_{17} \text{ pc}$.

4.2. Morphology

G328.4+0.2 is an extended Galactic source with a filled-center morphology, significant linear polarization across most of its extent, and a spectral index much flatter than for a typical shell-type supernova remnant. Down to our surface brightness limit, there is no evidence that G328.4+0.2 is surrounded by a larger, limb-brightened shell. This limit is sufficient to detect the shell of a typical young SNR (see Frail et al. 1995), although not sensitive enough to detect the shell component of the composite SNR G322.5-0.1 (Whiteoak 1992). Thus while the limits on a shell around G328.4+0.2 are not as stringent as around some other such sources, from the available data we class it as a Crab-like SNR.

The mere presence of a Crab-like or composite SNR is usually taken to indicate that there is an energetic pulsar within, even though in most such sources no pulsar has yet been detected. While indeed no pulsar has been seen within G328.4+0.2 in either radio waves (Manchester, D'Amico, & Tuohy 1985; Kaspi et al. 1996) or in X-rays (Wilson 1986; Hughes, Slane, & Plucinsky 2000), this can easily be accounted for by unfavorable beaming, insufficient sensitivity at the SNR's large distance, and significant scattering, dispersion (at radio wavelengths) and absorption (in X-rays) along the long line of sight. We thus assume in further discussion that there is an unseen rotation-powered pulsar within G328.4+0.2, whose relativistic wind powers the radio emission from the remnant.

The bar running through the center of G328.4+0.2 is a feature similar to that seen in many other Crab-like SNRs. There are two interpretations of such a feature: one is that it corresponds to a trail of emitting particles left behind by a pulsar with a

significant space velocity (e.g. Frail et al. 1996; Sun, Wang, & Chen 1999), the other is that the bar is actually comprised of two opposed jet-like features, produced by a bipolar outflow from the pulsar (e.g. Fürst et al. 1988, 1989). High-resolution X-ray imaging is required to distinguish between these possibilities, since the much shorter synchrotron lifetime of X-ray emitting particles will result in X-ray emission being concentrated around the current point of injection into the SNR. So if the bar is a high velocity pulsar leaving a trail, we expect to see X-ray emission concentrated at one end of the bar, while if it is a pair of outflows, X-ray emission should peak near the center of the bar.

4.3. Physical Properties

We first determine the radio luminosity, L_R , of G328.4+0.2. Hughes et al. (2000) demonstrate that any break in the continuum spectrum of this source is at a frequency higher than 100 GHz. We thus assume that the radio spectrum of G328.4+0.2 is a single power-law of spectral index $\alpha = -0.12$. Integrating between 100 MHz and 100 GHz, we then find a broad-band radio luminosity for G328.4+0.2 of $L_R = 3.3d_{17}^2 \times 10^{35} \text{ erg s}^{-1}$.

In Table 2, we compare the size and radio luminosity of G328.4+0.2 to those of other Crab-like SNRs (as well as Crab-like cores of composite SNRs) with similar properties; it can be seen that G328.4+0.2 is one of the most radio-luminous and largest Crab-like SNRs yet discovered. Two sources closely resemble G328.4+0.2: N157B (Wang & Gotthelf 1998; Lazendic et al. 2000), a Crab-like SNR in the Large Magellanic Cloud (LMC) in which a 16-ms X-ray pulsar has recently been discovered⁶, and G74.9+1.2 (Weiler & Shaver 1978; Wallace et al. 1997), a Galactic SNR which as yet has had no pulsar detected in it. Below we will argue that these three SNRs constitute a particular sub-class of Crab-like SNR.

A pulsar's spin-down luminosity is given by

$$\dot{E} \equiv 4I\pi^2\dot{P}/P^3, \quad (1)$$

where P is the period of the pulsar and $I = 10^{45} \text{ g cm}^{-2}$ is its moment of inertia. Defining $\epsilon = L_R/\dot{E}$, we find that in the few cases where a pulsar has been detected within a Crab-like SNR, the radio luminosity of the SNR normally falls in the narrow range $\epsilon = (1-5) \times 10^{-4}$ (Frail & Scharringhausen 1997; Gaensler et al. 2000). In particular, the Crab Nebula has $\epsilon = 4 \times 10^{-4}$, and we assume a similar value for G328.4+0.2. One then finds that its central pulsar has $\dot{E}_{38} = 8.3$ (where $\dot{E} = 10^{38}\dot{E}_{38} \text{ erg s}^{-1}$), a value consistent with that derived by Hughes et al. (2000) from the X-ray properties of this source. This value of \dot{E} ranks amongst the highest values seen for the radio pulsar population, and makes this source a good candidate for pulsed emission searches by future X-ray and γ -ray missions.

A pulsar drives a supersonic bubble into its surroundings, whose radius, R , is given by (Weaver et al. 1977; Arons 1983):

$$R = 0.82\dot{E}_{38}^{1/5}t_3^{3/5}n_0^{-1/5} \text{ pc}, \quad (2)$$

where $t_3 \text{ kyr}$ is the age of the pulsar and $n_0 \text{ cm}^{-3}$ is the density of the ambient medium. It is usually assumed that Crab-like SNRs are propagating into a low density component of the ISM (Chevalier 1977), for which we adopt a typical density

⁶The pulsar has so far remained undetected in radio waves, but otherwise has properties typical of a radio pulsar (Crawford et al. 1998).

$n_0 = 0.003 \text{ cm}^{-3}$. We can then determine an age for G328.4+0.2 of $t_3 \approx 7d_{17}^{5/3} \text{ kyr}$.

For a idealized braking index $n = 3$ and an initial period $P_i \ll P$, the age of the SNR is equal to its pulsar's characteristic age, $\tau_c \equiv P/2\dot{P}$. We can then combine our inferred age with Equation (1) to determine parameters for the pulsar of $P = 11 \text{ ms}$ and $B \equiv 3.2 \times 10^{19} (PP)^{1/2} \text{ G} = 6 \times 10^{11} \text{ G}$, where B is the inferred surface magnetic field of the neutron star, assuming a dipole geometry. These inferred parameters, along with the results of similar calculations for G74.9+1.2 and N157B, are given in Table 2 – we find that all three pulsars are of much smaller period, lower magnetic field and larger age than the Crab Pulsar.

Various assumptions have gone into the calculations behind this last statement, and we now consider what effect each one has on the results. The assumption least likely to be true is that $t = \tau_c$; if we relax this requirement to include braking indices $n \neq 3$ and initial periods $P_i \approx P$, we still find, for a wide range of parameters, that $\tau_c \gtrsim 0.7t$ (see Fig 3 of Marshall et al. 1998).

Since $P \propto \tau_c^{-1/2}$ and $B \propto \tau_c^{-1}$, the consequent inferred spin periods and magnetic fields are still significantly smaller than for the Crab Pulsar. A second assumption is that $\epsilon = \epsilon_{\text{Crab}}$; however the dependence on ϵ is even weaker than on τ_c ($P \propto \epsilon^{1/3}$ and $B \propto \epsilon^{1/6}$), so that even invoking a value of ϵ ten times larger than that for the Crab (which would be higher than for any pulsar observed) has little effect on the results. We have also assumed a value $n = 0.003 \text{ cm}^{-3}$; a significantly lower density than this can indeed produce a more typical magnetic field ($B \propto n^{-2/3}$), but still requires a fast period ($P \propto n^{-1/6}$). Meanwhile, Equation (2) is only strictly true for constant \dot{E} . In reality, \dot{E} will decrease as a function of time, so that the radius of the pulsar wind bubble will be larger than given by Equation (2) and will hence cause us to over-estimate the age of the system. While this effect is difficult to quantify, the ages given in Table 2 would have to be too large by a factor of 5–10 to produce periods as slow as that of the Crab Pulsar. Finally, we note that the calculations we have made for G328.4+0.2 all use the lower limit on the distance derived in Section 4.1; at greater distances, the inferred period and magnetic field are both even lower than those given in Table 2.

Thus even if not all of the assumptions which we have made are valid, one is still forced to conclude that the pulsars powering these SNRs are likely to be spinning rapidly and have low magnetic fields. In particular, the pulsar actually observed within N157B indeed fulfils this prediction, having observed properties quite similar to those we have inferred for it (see Table 2).

5. CONCLUSIONS

Our radio observations of G328.4+0.2 confirm it to be a Crab-like SNR at a distance of $>17 \text{ kpc}$, making it the largest and most radio-luminous such object in our Galaxy. G328.4+0.2, together with the Galactic SNR G74.9+1.2 and N157B in the LMC, appear to form a small subset of Crab-like SNRs with both high radio luminosities and large diameters. The high luminosities of these remnants demand a high value of \dot{E} for their central pulsars, while these remnants' large extent, even assuming an energetic pulsar and a low ambient density, requires them to be significantly older than the Crab Nebula. Since $\dot{E}\tau_c \propto P^{-2}$ and $\dot{E}\tau_c^2 \propto B^{-2}$, this combination of a high \dot{E} and large age can only be produced by a pulsar which is spinning at least twice as fast as the Crab Pulsar, but which has a magnetic field ~ 5 times weaker. Specifically, we infer G328.4+0.2 to be $\sim 7000 \text{ yrs}$ old and powered by a pulsar with period $P \approx 11 \text{ ms}$ and dipole magnetic field $B = 6 \times 10^{11} \text{ G}$. Similar properties are predicted for G74.9+1.2 and for N157B, which in the latter case agree with those of the pulsar recently detected within this SNR.

Using the distribution of pulsar initial magnetic fields proposed by Stollman (1987), we can estimate that the birth-rate of pulsars with magnetic fields $B \sim 6 \times 10^{11} \text{ G}$ is a fraction 0.05 of that of pulsars with magnetic fields comparable to the Crab Pulsar. Thus of the ~ 35 Crab-like and composite SNRs known in the Galaxy, we can expect ~ 2 to be powered by such low-field pulsars, and G328.4+0.2 and G74.9+1.2 may thus represent the complete sample of such sources.

The radio beaming fraction for young pulsars is estimated to be in the range 50–70% (Frail & Moffett 1993; Brazier & Johnston 1999). Thus the failure to detect radio pulsations from G328.4+0.2, G74.9+1.2 and N157B (Kaspi et al. 1996; Lorimer, Lyne, & Camilo 1998; Crawford et al. 1998) is unlikely to be solely due to beaming, and more likely results from the large distance to these objects. With continuing improvements in sensitivity, searches for pulsations towards these sources should eventually be successful.

We thank Taisheng Ye for early assistance with this project, and Pat Slane and Jack Hughes for useful discussions on the manuscript. We also acknowledge some important suggestions made by the referee, Roger Chevalier. The Australia Telescope is funded by the Commonwealth of Australia for operation as a National Facility managed by CSIRO. B.M.G. acknowledges the support of NASA through Hubble Fellowship grant HF-01107.01-98A awarded by the Space Telescope Science Institute, which is operated by the Association of Universities for Research in Astronomy, Inc., for NASA under contract NAS 5-26555. J.R.D. acknowledges a Visitor's Fellowship from the Netherlands Scientific Organization (NWO) during his stay at the NFRA.

REFERENCES

- Arons, J. 1983, *Nature*, 302, 301.
 Braz, M. A. & Epchtein, N. 1983, *Astr. Astrophys. Suppl. Ser.*, 54, 167.
 Brazier, K. T. S. & Johnston, S. 1999, *Mon. Not. R. astr. Soc.*, 305, 671.
 Caswell, J. L., Haynes, R. F., Milne, D. K., & Wellington, K. J. 1980, *Mon. Not. R. astr. Soc.*, 190, 881.
 Caswell, J. L., Murray, J. D., Roger, R. S., Cole, D. J., & Cooke, D. J. 1975, *Astr. Astrophys.*, 45, 239.
 Chevalier, R. A. 1977, in *Supernovae*, ed. D. N. Schramm, (Dordrecht: Reidel), p. 53.
 Cohen, R. J., Masheder, M. R. W., & Caswell, J. L. 1995, *Mon. Not. R. astr. Soc.*, 274, 808.
 Crawford, F., Kaspi, V. M., Manchester, R. N., Lyne, A. G., Camilo, F., & D'Amico, N. 1998, in *Proceedings of the Elba Workshop: Neutron Stars and Supernova Remnants*, volume 69, *Memorie della Societa' Astronomica Italiana*, p. 951.
 Fich, M., Blitz, L., & Stark, A. A. 1989, *Astrophys. J.*, 342, 272.
 Frail, D. A., Giacani, E. B., Goss, W. M., & Dubner, G. 1996, *Astrophys. J.*, 464, L165.
 Frail, D. A., Kassim, N. E., Cornwell, T. J., & Goss, W. M. 1995, *Astrophys. J.*, 454, L129.
 Frail, D. A. & Moffett, D. A. 1993, *Astrophys. J.*, 408, 637.
 Frail, D. A. & Scharringhausen, B. R. 1997, *Astrophys. J.*, 480, 364.

- Frater, R. H., Brooks, J. W., & Whiteoak, J. B. 1992, *J. Electr. Electron. Eng. Aust.*, 12, 103.
- Fürst, E., Handa, T., Morita, K., Reich, P., Reich, W., & Sofue, Y. 1988, *Proc. Astr. Soc. Jap.*, 40, 347.
- Fürst, E., Hummel, E., Reich, W., Sofue, Y., Sieber, W., Reif, K., & Dettmer, R.-J. 1989, *Astr. Astrophys.*, 209, 361.
- Gaensler, B. M., Manchester, R. N., & Green, A. J. 1998, *Mon. Not. R. astr. Soc.*, 296, 813.
- Gaensler, B. M., Stappers, B. W., Frail, D. A., Moffett, D. A., Johnston, S., & Chatterjee, S. 2000, *Mon. Not. R. astr. Soc.*, . submitted.
- Helfand, D. J. & Becker, R. H. 1987, *Astrophys. J.*, 314, 203.
- Hughes, J. P., Slane, P. O., & Plucinsky, P. 2000, *Astrophys. J.*, . submitted.
- Kaspi, V. M., Manchester, R. N., Johnston, S., Lyne, A. G., & D'Amico, N. 1996, *Astron. J.*, 111, 2028.
- Kerr, F. J., Bowers, P. F., Jackson, P. D., & Kerr, M. 1986, *Astr. Astrophys. Suppl. Ser.*, 66, 373.
- Kerr, F. J. & Lynden-Bell, D. 1986, *Mon. Not. R. astr. Soc.*, 221, 1023.
- Lazentic, J. S., Dickel, J. R., Haynes, R. F., Jones, P. A., & White, G. L. 2000, *Astrophys. J.*, . submitted.
- Lorimer, D. R., Lyne, A. G., & Camilo, F. 1998, *Astr. Astrophys.*, 331, 1002.
- Manchester, R. N., D'Amico, N., & Tuohy, I. R. 1985, *Mon. Not. R. astr. Soc.*, 212, 975.
- Manchester, R. N. & Taylor, J. H. 1977, *Pulsars*, (San Francisco: Freeman).
- Marshall, F. E., Gotthelf, E. V., Zhang, W., Middleditch, J., & Wang, Q. D. 1998, *Astrophys. J.*, 499, L179.
- Mills, B. Y., Slee, O. B., & Hill, E. R. 1961, *Aust. J. Phys.*, 14, 497.
- Milne, D. K., Goss, W. M., Haynes, R. F., Wellington, K. J., Caswell, J. L., & Skellern, D. J. 1979, *Mon. Not. R. astr. Soc.*, 188, 437.
- Nomoto, K. 1987, in *The Origin and Evolution of Neutron Stars (IAU Symposium 125)*, ed. D. J. Helfand & J.-H. Huang, (Dordrecht: Reidel), 281.
- Reynolds, S. P. & Chevalier, R. A. 1984, *Astrophys. J.*, 278, 630.
- Sankrit, R. & Hester, J. J. 1997, *Astrophys. J.*, 491, 796.
- Shaver, P. A. & Goss, W. M. 1970, *Aust. J. Phys. Astr. Suppl.*, 14, 133.
- Stollman, G. M. 1987, *Astr. Astrophys.*, 178, 143.
- Sun, M., Wang, Z., & Chen, Y. 1999, *Astrophys. J.*, 511, 274.
- van Langevelde, H. J. & Cotton, W. D. 1990, *Astr. Astrophys.*, 239, L5.
- Wallace, B. J., Landecker, T. L., & Taylor, A. R. 1997, *Astron. J.*, 114, 2068.
- Wallace, B. J., Landecker, T. L., Taylor, A. R., & Pineault, S. 1997, *Astr. Astrophys.*, 317, 212.
- Wang, Q. D. & Gotthelf, E. V. 1998, *Astrophys. J.*, 494, 623.
- Weaver, R., McCray, R., Castor, J., Shapiro, P., & Moore, R. 1977, *Astrophys. J.*, 218, 377.
- Weiler, K. W. & Panagia, N. 1978, *Astr. Astrophys.*, 70, 419.
- Weiler, K. W. & Panagia, N. 1980, *Astr. Astrophys.*, 90, 269.
- Weiler, K. W. & Shaver, P. A. 1978, *Astr. Astrophys.*, 70, 389.
- Whiteoak, J. B. Z. 1992, *Mon. Not. R. astr. Soc.*, 256, 121.
- Whiteoak, J. B. Z. & Green, A. J. 1996, *Astr. Astrophys. Suppl. Ser.*, 118, 329.
- Wilson, A. S. 1986, *Astrophys. J.*, 302, 718.

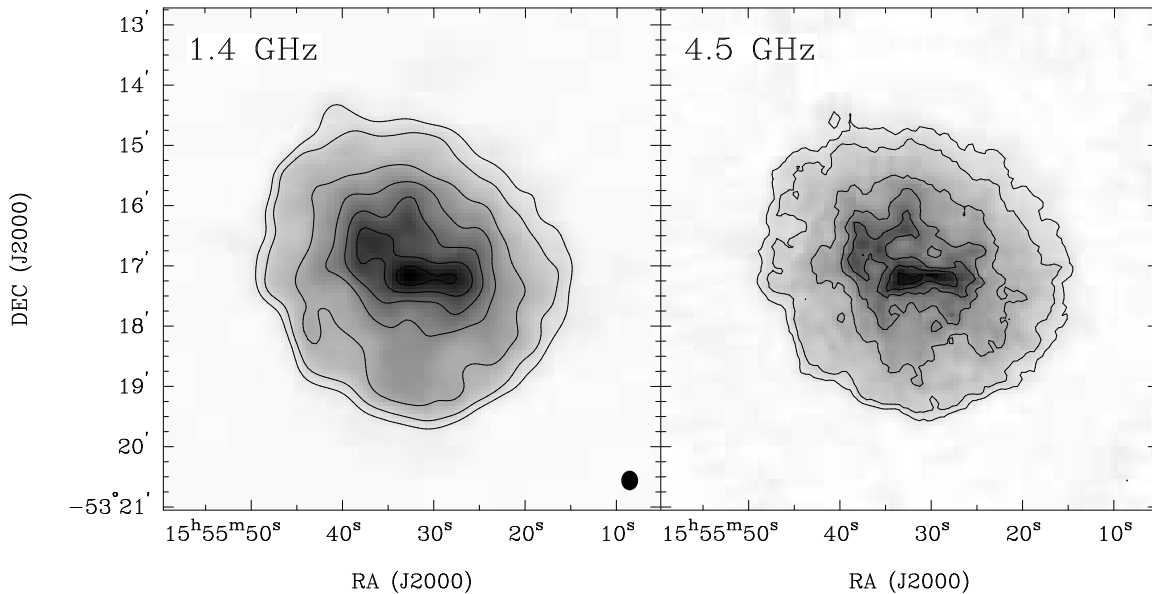


FIG. 1.— 1.4 and 4.5 GHz ATCA images of SNR G328.4+0.2, corrected for primary beam attenuation. The 1.4 GHz image has a greyscale which ranges from -5 to $200 \text{ mJy beam}^{-1}$, with contour levels at 15, 30, 60, ..., 150, 180 mJy beam^{-1} . The 4.5 GHz image ranges from -0.05 to $2.0 \text{ mJy beam}^{-1}$, with contours at levels of 0.15, 0.30, 0.60, ..., 1.50, 1.80 mJy beam^{-1} . The synthesized beam is shown at the lower right of each panel.

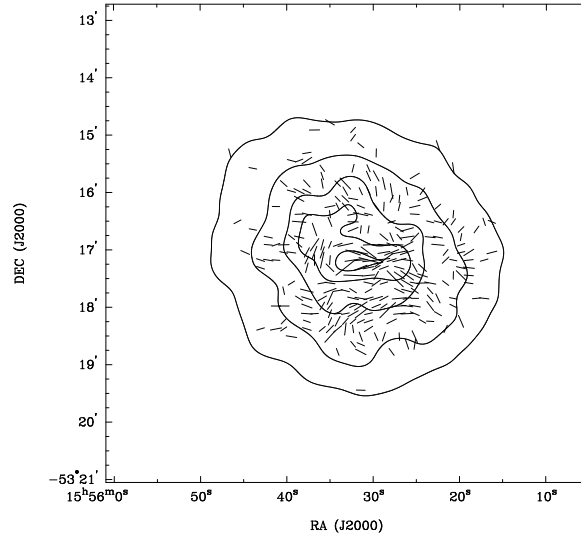


FIG. 2.— Linearly polarized emission from G328.4+0.2 at 4.5 GHz. The length of each vector represents the polarized intensity at that position, while the position angle corresponds to the orientation of the electric field vector when averaged across the entire 4.5 GHz band. The longest vector in the image is for a polarized intensity of $0.6 \text{ mJy beam}^{-1}$. The contours represent total intensity at 4.5 GHz, smoothed to a resolution of $20''$.

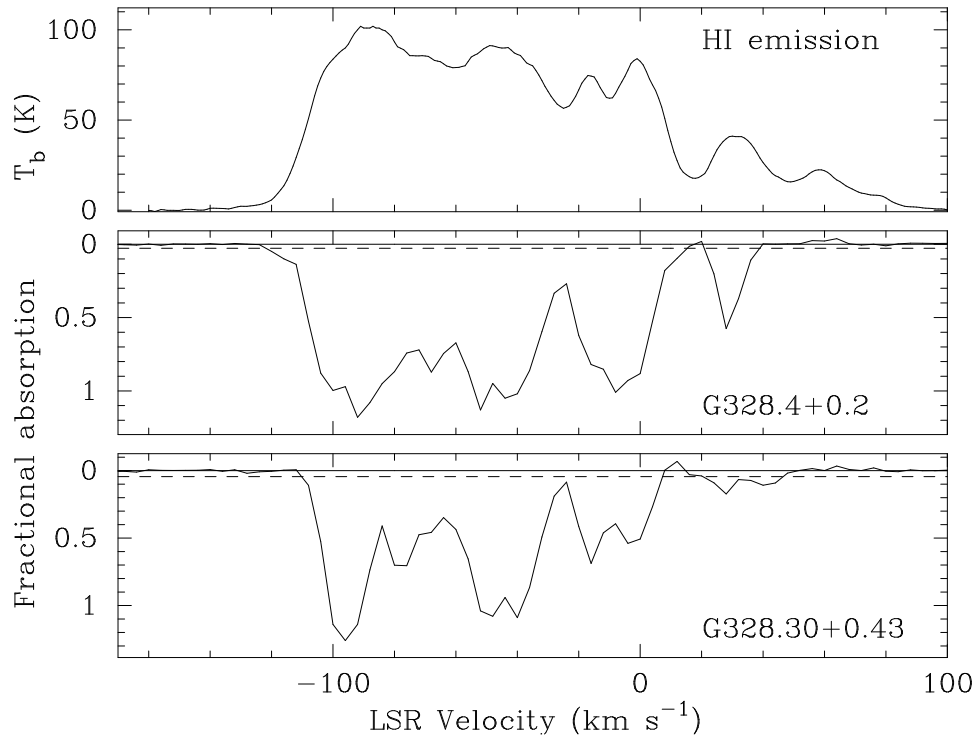


FIG. 3.— H I emission and absorption in the region. The upper panel shows the H I emission spectrum measured by Kerr et al. (1986) in the direction $l = 328.5$, $b = 0.25$. The central panel shows H I absorption towards SNR G328.4+0.2, while the lower panel shows absorption towards the nearby H II region G328.30+0.43. The dashed lines in the absorption profiles correspond to absorption at levels of 6σ , where the rms has been computed from line-free channels.

TABLE 1
ATCA OBSERVATIONS OF G328.4+0.2.

	1.4 GHz	4.5 GHz	
Dates Observed	1999 July 31	1993 May 23, 1993 July 19, 1993 Sep 04, 1995 Jan 22, 1995 Feb 26	
Resolution	19''5 × 16''5	2''0 × 1''5	
rms noise (mJy beam ⁻¹)	0.8	0.04	(Stokes <i>I</i>)
	0.1	0.04	(Stokes <i>V</i>)
Flux density of G328.4+0.2 (Jy)	14.3 ± 0.1	12.5 ± 0.2	
Center of G328.4+0.2	15 ^h 55 ^m 33 ^s , -53°17'00'' (α , δ ; J2000)		
	328.42 +0.22 (<i>l</i> , <i>b</i>)		
Diameter of G328.4+0.2	5'0 × 5'0		

TABLE 2

PROPERTIES OF G328.4+0.2 AND TWO OTHER CRAB-LIKE SNRS OF COMPARABLE RADIO LUMINOSITIES AND DIAMETERS. THE CRAB NEBULA IS INCLUDED FOR COMPARISON.

SNR	L_R^1 (10 ³⁵ erg s ⁻¹)	Diameter (pc)	Properties of associated pulsar ²				Ref ³
			<i>P</i> (ms)	τ_c (kyr)	\dot{E} (10 ³⁸ erg s ⁻¹)	<i>B</i> (10 ¹² G)	
G328.4+0.2	3.3	25	11	7	8.3	0.6	1
G74.9+1.2	0.7	25	18	11	1.8	0.7	2
N157B (observed)	3.5	24	16	5	4.8	0.9	3, 4
N157B (inferred)	"	"	11	6	8.8	0.6	
Crab Nebula	1.8	3.5	33	0.9	4.5	3.8	2, 5

¹Integrated between 100 MHz and 100 GHz.

²No pulsar has yet been detected in G328.4+0.2 or G74.9+1.2, and the properties given here have been inferred using the method described in the text. For N157B, both inferred and actual pulsar properties are listed.

³References: (1) this paper; (2) Helfand & Becker (1987); (3) Marshall et al. (1998); (4) Lazendic et al. (2000); (5) Manchester & Taylor (1977)